IV International Conference on Particle-based Methods – Fundamentals and Applications
PARTICLES 2015
E. Oñate, M. Bischoff, D.R.J. Owen, P. Wriggers & T. Zohdi (Eds)

TRIBOLOGICAL EFFECTS IN GRANULAR MATERIALS AND THEIR IMPACT ON THE MACROSCOPIC MATERIAL BEHAVIOUR

Bettina Suhr[1] **and Klaus Six**[1]

[1] Virtual Vehicle Research Center
Inffeldgasse 21/A, A-8010 Graz, Austria
bettina.suhr@v2c2.at, klaus.six@v2c2.at, http://www.v2c2.at

Key words: Tribology, Direct Shear Test, Granular Materials, DEM, Friction

Abstract. In the discrete element simulation of granular materials, the modelling of contacts is crucial for the macroscopic material behaviour. From the tribological point of view, friction at contacts needs to be modelled carefully, as it depends on several factors, e.g. contact normal load or temperature to name only two. In discrete element method (DEM) simulations the usage of Coulomb's law of friction is state of the art. It reduces all tribological effects to only one constant coefficient of friction. Motivated by research on wheel-rail contacts, a pressure dependency of the interparticle coefficient of friction is introduced in a new DEM model. Direct shear tests are conducted on steel spheres of a certain size distribution. The strong influence of interparticle friction on the bulk friction is shown via a variation of the constant interparticle friction coefficient. Simulations with constant and pressure dependent interparticle friction are compared. For the pressure dependent interparticle friction a pressure dependency of the bulk friction is seen which matches qualitatively the behaviour known from testing reported in literature.

1 INTRODUCTION

Solid like granular materials generally comprise a high number of particle-particle and particle-environment contacts. The frictional behaviour of these contacts has a high influence on the macroscopic behaviour of the material. In the sense of a tribological system friction is influenced by several parameters like contact normal load, relative motion, surface roughness, contact temperature and contact conditions (dry, wet, lubricated contact conditions, etc.).

The discrete (distinct) element method (DEM) was introduced by Cundall and Strack, see [1], and has become a widely used tool for modelling the mechanical behaviour of solid-like granular materials. While there are several topics of active research regarding DEM, it is state of the art to consider the frictional behaviour of contacts by application of Coulomb's law. At a contact the resulting contact force is decomposed in normal

and tangential direction, F_n and F_t, and contact laws for their calculation are chosen. In tangential direction the force which can be transferred is bounded. This bound has a high influence on the behaviour of the granular material and generally consists of a part depending on the normal force and a part representing cohesion (independent of the normal force). Coulomb's law is the simplest way to model the normal force dependent part of this bound. A constant interparticle friction coefficient, μ, is introduced, which describes the maximal allowed ratio between tangential and normal force. While the contact sticks, the ratio is strictly less than the coefficient of interparticle friction. When the ratio of tangential and normal force grows and equality is reached, the contact slides. During sliding the ratio remains constant. For cohesionless materials Coulomb's law can be written as follows:

$$F_t = min\left(\mu F_n, \tilde{F}_t\right) \ , \tag{1}$$

where $\tilde{F}_t$ is the pre-sliding shear force calculated using the contact constitutive model. Coulomb's law can also be stated using the internal friction angle, ϕ, which is connected to the interparticle friction coefficient by $\mu = \tan(\phi)$.

Frequently used tests for the investigation of the shear behaviour of granular materials are the triaxial test and the direct shear (or shear box) test. Usually the Mohr-Coulomb failure criterion is used which reads as:

$$\tau_f = \tan(\Phi)\sigma_n + c \ , \tag{2}$$

where τ_f is the final shear stress, Φ is the bulk friction angle and c is a material parameter representing cohesion of the granular material, i.e. $c = 0$ for cohesionless materials. The bulk friction angle of a granular material is an important characteristic for its shear behaviour. Alternatively the peak friction angle can be determined, where the maximal shear stress instead of the final one is used in equation (2).

In the literature there exist several works which state a strong influence of the interparticle friction on the bulk friction angle, see e.g. [2, 3, 4] who simulated direct shear tests and compared the results to experiments.

It is frequently stated that the bulk/peak friction angle of a granular medium is constant, i.e. independent of the normal stress. This result can be found e.g. in [3] or [4] who considered equi-sized steel balls and glass beads respectively. Direct shear test with different normal stresses were conducted. In the regime of applied normal stresses, in both works a linear relation between the measured shear stress and normal stress was found. Thus the application of the Mohr-Coulomb criterion was justified and the bulk friction angle was constant.

On the contrary, [4] states a clearly non-linear relation, i.e. pressure dependency, when the shear test is performed on paired glass beads instead of single glass beads. Here the applied normal stress ranges from 3 kPa to 24 kPa and a dependency of the bulk friction angle on these pressures can be seen. In [5] the same experimental results are

compared to DEM simulation. The pressure dependency of the bulk friction angle found in the experimental results could not be reproduced in the DEM simulations which used a constant interparticle friction coefficient for all load cases.

Similar experimental results regarding a pressure dependency of the bulk friction angle are found in [6] where railway ballast is investigated in direct shear tests. The normal stress is varied between 15 kPa and 75 kPa and a nonlinear dependency between shear stress and normal stress is shown. Here also several works on rock-fill materials are cited which state a non-linear relationship which is significant at low normal stresses and gradually reduces as the normal stress increases.

This description matches well with the results of [7]. A pressure dependent coefficient of friction between smooth silo walls and particles was found for small normal stresses. It seems that depending on the considered material and particle shape a non-linear relation between bulk friction angle and normal stress can be observed for low normal stresses.

Motivated by the above experimental findings on granular media and results obtained on the wheel-rail contact for steel, the authors will use a non-constant coefficient of friction in DEM simulations. In simulations of direct shear tests, the application of this law will result in a non-linear dependency of the bulk friction angle on the normal stress.

2 PRESSURE DEPENDENT FRICTION COEFFICIENT

Investigations on the frictional behaviour of wheel-rail contacts (steel-steel) showed that the assumption of a constant coefficient of friction is not sufficient to reproduce results observed at experiments, see e.g. [8]. In Figure 1 results of High Pressure Torsion tests (HPT) are shown. In a HPT test two steel discs are rotated against each other, while the normal stress, σ_n and the shear stress, τ, are measured. In this case the ratio between τ and σ_n is the coefficient of friction. From Figure 1(a) to 1(b) the maximum normal stress σ_n is doubled. If the coefficient of friction was constant, then $\frac{\tau}{\sigma_n}$ would be constant and thus τ would be doubled. In Figure 1(b) it can be seen that the τ is clearly

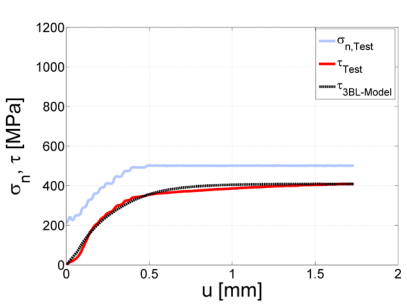

(a) normal stress $\sigma_n = 500$ MPa.

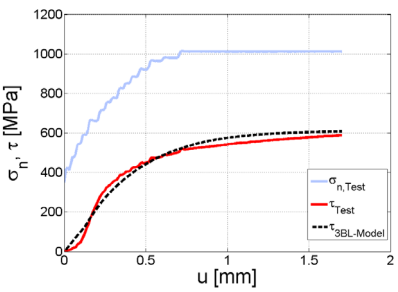

(b) normal stress $\sigma_n = 1000$ MPa.

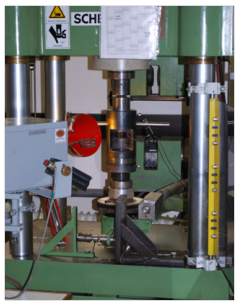

(c) HPT test rig.

Figure 1: High Pressure Torsion (HPT) tests where two steel-discs are rotated against each other; measurement of normal stress (σ_n) and shear stress (τ) over displacement u; increasing normal stress reduces ratio τ/σ_n, comparison to results from model [8].

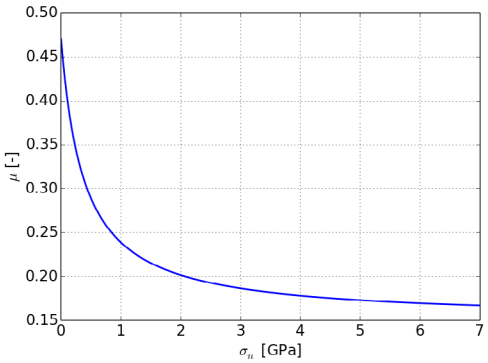

Figure 2: Graph of the pressure dependent coefficient of friction as defined in Equation (3).

lower and therefore a significant dependency of the coefficient of friction on the normal load can be concluded from the experiments.

Similar results as in [8] are also obtained in [9] from Popov et. al. With the method of Movable Cellular Automata (MCA) the wheel-rail contact is modelled (steel-steel) and from simulation results a normal pressure dependent coefficient of friction is derived:

$$\mu(\sigma_n) = 0.15 + \frac{0.3243}{1 + 0.00212\frac{\sigma_n E}{\sigma_0}} \,, \tag{3}$$

where σ_n is the applied normal stress, E is the Young modulus, $E = 206\ GPa$, and σ_0 is the ultimate strength and was varied between 92 and 552 MPa. The graph of the above function is plotted in Figure 2 for $\sigma_0 = 400$ MPa.

This pressure dependent coefficient of friction will be used in the following DEM simulations. For the contact forces the frequently used Hertz-Mindlin no slip contact model will be used, compare e.g. [10]. In normal direction of the contact the Hertz model is as follows:

$$F_n = \frac{4}{3}\hat{E}\sqrt{\hat{R}}\sqrt{u_n^3} \,, \tag{4}$$

where $\hat{E}$ is the equivalent Young modulus of the contact, $\hat{R}$ is the equivalent contact radius and u_n is the overlap in normal direction. In the Hertzian contact model the area of contact is circular (sphere-sphere contact), therefore an averaged pressure, $\bar{\sigma}_n$ can be calculated by dividing the contact force by the contact area.

$$\bar{\sigma}_n := \frac{F_n}{a^2\pi} = \frac{F_n}{\pi}\left(\frac{4\hat{E}}{3F_n\hat{R}}\right)^{\frac{2}{3}} \,, \tag{5}$$

where $a = \left(\frac{3F_n\hat{R}}{4\hat{E}}\right)^{\frac{1}{3}}$ is the radius of the contact patch. In the tangential direction of the contact the Mindlin no slip model is applied. The trial or pre-sliding shear force is denoted by $F_{t,t}$ and can be calculated as:

$$F_{t,t} = 8\,a\,\hat{G}\,u_s\ , \tag{6}$$

where $\hat{G}$ is the equivalent shear modulus and u_s the shear displacement. Using the constant coefficient of friction, the shear force is given by:

$$F_t = \begin{cases} F_{t,t} & \text{if } F_{t,t} \leq \mu F_n \\ \mu F_n & \text{otherwise} \end{cases}\ . \tag{7}$$

For the use of the pressure dependent friction coefficient, we now change Equation (7) to:

$$F_t = \begin{cases} F_{t,t} & \text{if } F_{t,t} \leq \mu(\bar{\sigma}_n) F_n \\ \mu(\bar{\sigma}_n) F_n & \text{otherwise} \end{cases}\ , \tag{8}$$

where $\bar{\sigma}_n$ is given by Equation (5) and $\mu(\bar{\sigma}_n)$ by Equation (3).

3 DEM SIMULATION OF DIRECT SHEAR TESTS

The influence of interparticle friction on the macroscopic behaviour will be investigated via simulation of direct shear tests. Results of a variation of the constant friction coefficient will be compared to those obtained with the above introduced pressure dependent friction coefficient.

All simulations are conducted with the DEM software Yade, [11]. In this software the soft contact approach is used together with explicit discretization in time. As already mentioned the main focus of this work is the modification of the tangential contact law, regarding the friction coefficient. The basis for this work is the Hertz-Mindlin no-slip contact model as given in Equations (4, 7) . If the modified contact law, (4, 8), is used, it will be stated explicitly.

The setup of a direct shear test is shown in Figure 3(a). The lower box has the dimensions 0.3 m × 0.3 m × 0.1 m and the upper box 0.3 m × 0.3 m × 0.2 m. For all shear tests non-uniform sizes of steel spheres are used. These sphere samples all share the same size distribution, which can be seen in Figure 3(b). The material of the spheres and the walls of the shear box is assumed to be equal. The material parameters of steel used in the DEM simulation are summarized in Table 1.

For sample generation 6000 spheres of the mentioned size distribution are randomly placed in a box above the shear box. Then the spheres fall under the influence of gravity and are allowed to come to rest in the shear box. To achieve a dense packing the friction coefficient is set to 0 in this initial phase of the simulation. For a reduction of computational time the gravity force is enlarged by factor 5. When the spheres came to rest, a steel plate is inserted above the spheres, the friction coefficient is increased to 0.2 and gravity force is set to its original value. Now the normal load is applied on the spheres using a servo control mechanism (P-control). After the specified normal load is reached and the spheres are at rest, the shearing phase starts by imposing a velocity on the lower

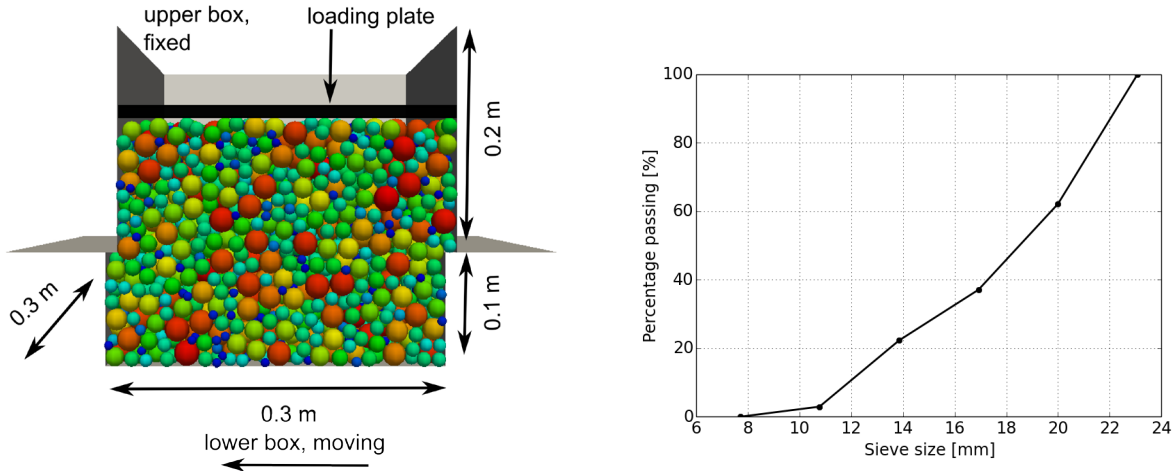

(a) Setup of shear box test.

(b) Size distribution of spheres.

Figure 3: Details on shear box test and size distribution of spheres.

shear box. Variations of the shear velocity showed that shearing with 1 $\frac{mm}{s}$ yielded results which can be considered quasi-static, i. e. a lower shearing rate yielded the same result.

The direct shear test will be simulated with three different levels of applied normal stress, σ_n = 75 kPa, 225 kPa and 375 kPa. At first the interparticle friction coefficient is constant, $\mu = 0.2$, and the Hertz-Mindlin no slip contact model (4, 7) is used. In Figure 4(a) the shear stress over the shear path is shown in the upper plot. For the calculation of the shear stress, all contact forces belonging to the lower box and the bottom are summed; then only the component in shear direction is divided by the cross-sectional area of the shear box 0.09 m^2. In the lower part of Figure 4(a) the porosity of the samples is plotted over the shear path. At the beginning of all three tests there is a short phase where the samples are compressed, while dilation occurs for the rest of the simulation. Due to problems with the control of the applied normal stress at the beginning of the simulations sometimes kinks in the shear stress can be seen. As the duration of these problems is usually very small, the effect on the overall response of the bulk material is negligible.

To check the influence of the spheres' initial configuration on the simulation results, five different configurations were generated with the above described procedure. The results

Table 1: Parameters used in DEM simulations.

Parameter	Diameter	Density	Young modulus	Poisson's ratio	friction coefficient
Value	8 - 24 mm	7833.34 $\frac{kg}{m^3}$	200 GPa	0.28	0.2

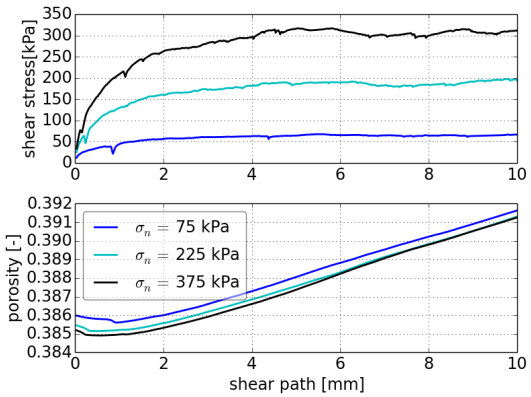

(a) Shear stress over shear displacement.

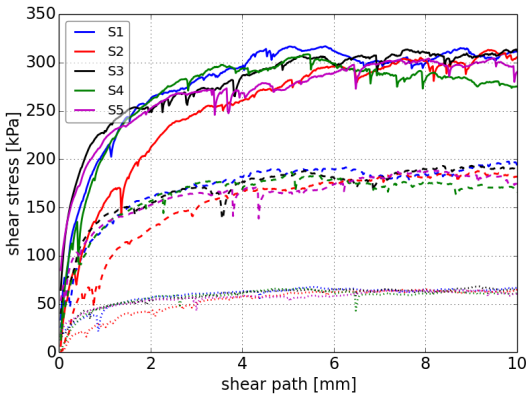

(b) Influence of initial configuration. Solid lines: $\sigma_n = 375$ kPa, dashed lines: $\sigma_n = 225$ kPa, dotted lines: $\sigma_n = 75$ kPa

Figure 4: Simulation results for direct shear tests with constant interparticle friction $\mu = 0.2$.

can be seen in Figure 4(b). The different initial settings are named S1 till S5. It can be seen that S2 has a lower initial slope than the other settings and S4 has the smallest final shear stress for all three levels of applied normal stress. It seems that for the chosen size distribution of the spheres the sample generation method can not ensure similar initial packings. Also differences in the initial porosity of the settings occur, which lie between 0.383 and 0.386. The maximal deviations in the final shear stress are 3 % for $\sigma_n = 75$ kPa, 11 % for $\sigma_n = 225$ kPa and 9 % for $\sigma_n = 375$ kPa. Obviously, to some extent the same problems would occur if tests in the lab were conducted. Nevertheless the reduction of these deviation via a different method for sample generation will be future work. For the time being, influences off the different initial settings will be reported, where they are of interest.

3.1 Influence of constant interparticle friction coefficient

It is well known that interparticle friction is a key factor for the shear behaviour of granular materials. In the following the interparticle friction coefficient will be varied between 0.1 and 0.4 to investigate its influence on the bulk friction angle for one considered initial setting. From the conducted simulations the final shear stress is calculated as the median of the last hundred readings of the shear stress (over a shear path of 2 mm). Here the median instead of the mean value is chosen due to its insensitivity with respect to outliers. Figure 5(a) shows the resulting final shear stresses, τ_f, over the applied normal stress, σ_n, for the different values of the interparticle friction coefficient. The already mentioned Mohr-Coulomb criterion for cohesionless material is used and the least squares fit for each value of interparticle friction is shown. The slope of these lines is the tangent of

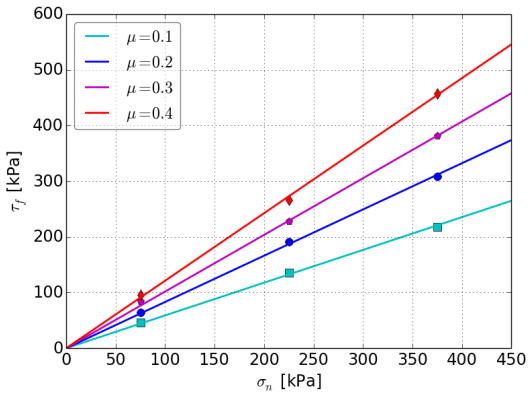

(a) Final shear stress, τ_f, over applied normal stress, σ_n.

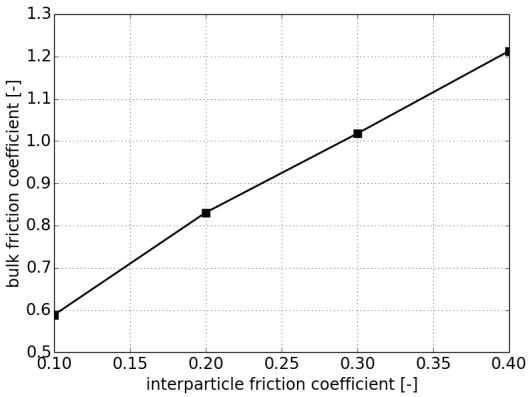

(b) Bulk friction coefficient over interparticle friction coefficient.

Figure 5: Influence of (constant) interparticle friction on bulk friction.

the bulk friction angle and will be denoted here as bulk friction coefficient. In Figure 5(b) this bulk friction coefficient is plotted over the interparticle friction coefficient.

The Mohr-Coulomb criterion states a linear relation between normal stress and final shear stress. The obtained bulk friction coefficient shows no pressure dependency. The simulation results obtained with constant interparticle friction coefficients agree well with the linear Mohr-Coulomb criterion. Thus, it can be concluded that constant interparticle friction can not be used to obtain a pressure dependency in bulk friction.

The strong influence of interparticle friction on the bulk friction coefficient is well shown with the presented results.

3.2 Usage of pressure dependent interparticle friction

As a next step simulations with the pressure dependent interparticle friction coefficient, (3) from [9], together with the modified shear force law (8) are presented. The results will be compared to simulations using $\mu = 0.2$. In the model of pressure dependent interparticle friction, the Young modulus is set to $E = 200$ GPa. For the ultimate strength, σ_0, the interval of 92 to 552 MPa is specified in [9]. In this work $\sigma_0 = 400$ MPa is used. In Figure 6(a) the normalized shear stress $\frac{\tau}{\sigma_n}$ is plotted over the shear path for $\mu = 0.2$ and the pressure dependent friction coefficient, μ pdf. Considering $\sigma_n = 375$ kPa in the lower plot, then the simulation results for $\mu = 0.2$ and pressure dependent μ coincide (calibration of the model via σ_0). In the upper plot, where $\sigma_n = 75$ kPa , $\frac{\tau_f}{\sigma_n}$ is about 10 % larger for for pressure dependent μ than for $\mu = 0.2$. For the pressure dependent μ the bulk friction coefficient decreases with increasing σ_n until it coincides at $\sigma_n = 375$ kPa with the value obtained with $\mu = 0.2$, compare Figure 6(a). Thus, the pressure dependency which is introduced in interparticle friction is also seen in the resulting bulk friction coefficient.

This behaviour of the bulk friction coefficient qualitatively agrees with observations from direct shear experiments reported in literature.

The pressure dependency in bulk friction, caused by the pressure dependency in interparticle friction, is in a similar range than the scatter of results caused by the different initial settings, compare Figure 4(b). A comparison of the simulations using $\mu = 0.2$ and pressure dependent μ for all five initial settings is done. In Figure 6(b) the bulk friction coefficient is calculated for each simulation individually. The solid bars show the bulk friction for the simulations with $\mu = 0.2$ and shaded bars belong to pressure dependent μ. While the extent of pressure dependency of the bulk friction coefficient varies between the initial settings it is present in all cases.

The authors would like to emphasize that it is not possible to use a higher (constant) friction coefficient and to obtain the same results as with pressure dependent μ. While it would be possible to chose a lower value for interparticle friction such that the final shear stress for $\sigma_n = 75$ kPa is met, then the final shear stress for $\sigma_n = 225, 375$ kPa would be too high.

For the simulation with pressure dependent μ and $\sigma_n = 75$ kPa the normal forces at the end of the test are plotted in Figure 7(a). For improved visibility only contacts with $F_n \geq 70$ N are displayed. With this threshold 10 % of all contact are plotted. On the same contacts the pressure dependent μ is shown in Figure 7(b). The friction coefficient lies between 0.189 and 0.23 at contacts with $F_n \geq 70$ N. As it can be seen in the plot, most contacts have larger friction coefficients than the value of 0.2 which was used for the comparison simulation. If all contacts are considered, then the maximal friction coefficient is 0.46.

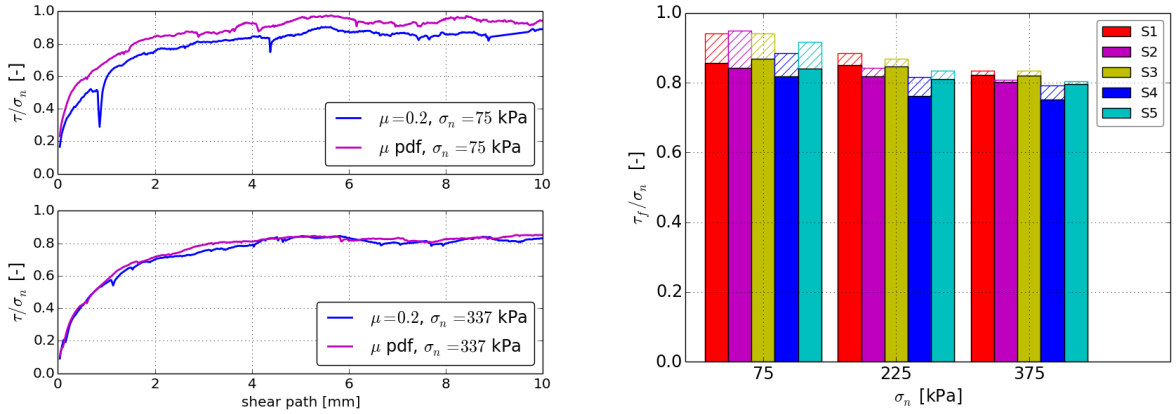

(a) Normalized shear stress over shear displacement. Comparison for $\sigma_n = 375$ kPa and $\sigma_n = 75$ kPa.

(b) Final shear stress divided by normal stress over applied normal stress for five different initial settings. Solid bars: $\mu = 0.2$, shaded bars: μ =pdf.

Figure 6: Comparison of constant interparticle friction and pressure dependent friction (pdf).

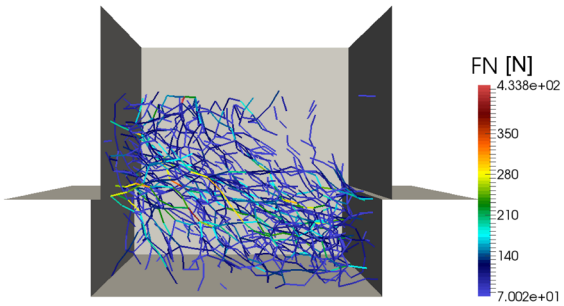

(a) Contact normal forces [N]. Only contacts with $F_n \geq 70$ N are displayed for improved visibility.

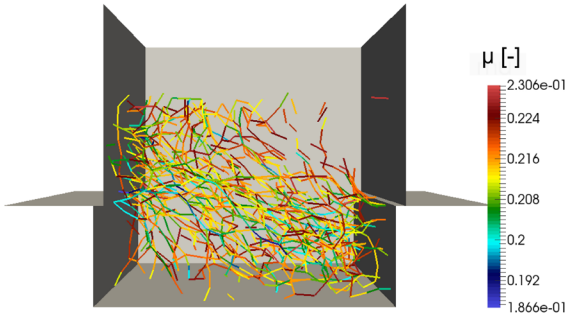

(b) Pressure dependent friction coefficient, plotted on contacts with $F_n \geq 70$ N.

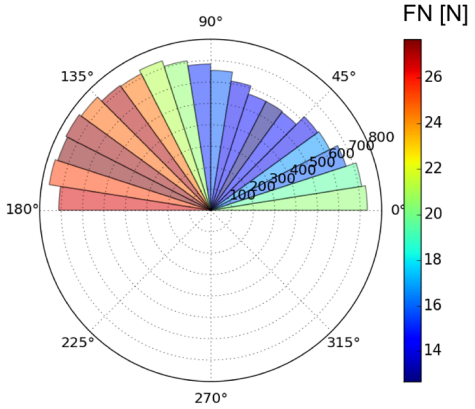

(c) Angular distribution of normal forces [N].

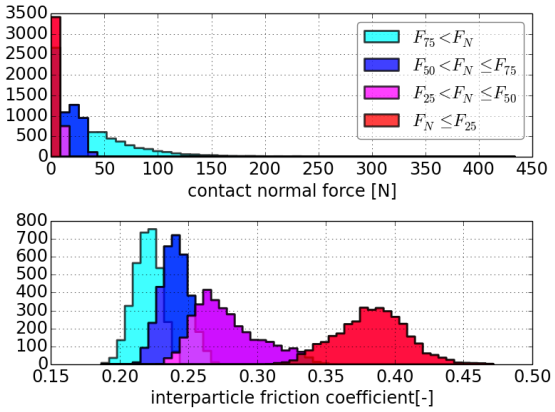

(d) Histogram of normal forces [N] and pressure dependent μ. The data is divided in four groups of equal size with ascending normal force.

Figure 7: Fabric analysis of simulation with pressure dependent friction coefficient and $\sigma_n = 75$ kPa at shear displacement 10 mm

The angular distribution of normal forces at sphere-sphere contacts is shown in Figure 7(c). The length of each bar represents the number of contacts in the corresponding direction and the colour of each bar stands for the averaged normal force. Note that the average forces are low as many contacts have very small normal forces. It can be seen that the contacts which carry the largest load are clearly directed.

In Figure 7(d) two histograms of the contact normal force and the pressure dependent μ are shown. The data is divided in four groups of equal size with ascending normal force. Each group contains 25 % of all contacts, so in the first group $F_n \leq F_{25}$, where F_{25} denotes the 25 % quantile of the data and so on. The upper histogram shows the normal force. Note that nearly half of the data (the first two groups) lies in the first bin, which illustrates the huge amount of contacts which carry nearly no load. In the lower histogram the corresponding values of the interparticle friction coefficient are plotted.

Low contact forces belong to high values of interparticle friction, as can be seen for the red and magenta data group. High contact forces result in lower interparticle friction. The values of the cyan data group lie in the same interval as those plotted in Figure 7(b). Note that overlaps between the data groups of the interparticle friction coefficient exist, as the contact's equivalents radius also enters its calculation.

4 CONCLUSIONS

In this contribution simulations of direct shear tests are conducted. The samples consist of steel spheres of a certain size distribution and are loaded at three different levels of normal stress, $\sigma_n = 75, 225, 375$ kPa. The influence of the spheres' initial configuration is rather strong. Comparing five different initial settings deviations in the final shear stress up to 11 % occur. To some extent this problem would also occur when experiments were conducted in the lab. The reduction of these deviations via a modification of the method for sample generation will be future work.

The strong influence of interparticle friction on the bulk friction of the granular material is shown via a variation of a constant interparticle friction coefficient. Motivated by results on the whee-rail contact of steel a newly developed pressure dependency of interparticle friction is introduced. Direct shear tests with pressure dependent interparticle friction and constant $\mu = 0.2$ are compared. The pressure dependency introduced in interparticle friction is clearly seen in the resulting bulk friction coefficient. Considering one initial setting and $\sigma_n = 75$ kPa, then the bulk friction coefficient is about 10 % larger for pressure dependent μ than for $\mu = 0.2$. For the pressure dependent μ the bulk friction coefficient decreases with increasing σ_n until it coincides at $\sigma_n = 375$ kPa (where the model was calibrated) with the value obtained with $\mu = 0.2$. Due to the scatter of results with different initial configurations it is difficult to quantify the effect on the bulk friction coefficient in general. Nevertheless the pressure dependency in bulk friction is – to different extent – seen for all five initial settings. Qualitatively these results matches the behaviour observed in testing reported in literature.

ACKNOWLEDGMENTS

The authors gratefully acknowledge funding of the Austrian Science Fund (FWF) for the project P 27147-N30: Short- and Long-Term Behaviour of Solid-Like Granular Materials.

VIRTUAL VEHICLE Research Center is funded within the COMET – Competence Centers for Excellent Technologies – programme by the Austrian Federal Ministry for Transport, Innovation and Technology (BMVIT), the Federal Ministry of Science, Research and Economy (BMWFW), the Austrian Research Promotion Agency (FFG), the province of Styria and the Styrian Business Promotion Agency (SFG). The COMET programme is administrated by FFG.

REFERENCES

[1] P. A. Cundall and O. D. L. Strack. A discrete numerical model for granular assemblies. *Gotechnique*, 29(1):47 65, 1979.

[2] Q. Ni, W. Powrie, X. Zhang, and R. Harkness. *Effect of Particle Properties on Soil Behavior: 3-D Numerical Modeling of Shearbox Tests*, chapter 4, pages 58–70. Numerical Methods in Geotechnical Engineering. 2000.

[3] L. Cui and C. O'Sullivan. Exploring the macro- and micro-scale response of an idealised granular material in the direct shear apparatus. *Geotechnique*, 56:455–468(13), 2006.

[4] Johannes Härtl and JinY. Ooi. Experiments and simulations of direct shear tests: porosity, contact friction and bulk friction. *Granular Matter*, 10(4):263–271, 2008.

[5] Johannes Härtl and Jin Y. Ooi. Numerical investigation of particle shape and particle friction on limiting bulk friction in direct shear tests and comparison with experiments. *Powder Technology*, 212(1):231–239, Sep 2011.

[6] Buddhima Indraratna, Ngoc Trung Ngo, and Cholachat Rujikiatkamjorn. Behavior of geogrid-reinforced ballast under various levels of fouling. *Geotextiles and Geomembranes*, 29(3):313 – 322, 2011.

[7] U Tuzun and O R Walton. Micro-mechanical modelling of load dependent friction in contacts of elastic spheres. *J. Phys. D: Appl. Phys.*, 25(1A):A44, 1992.

[8] K. Six, A. Meierhofer, G. Müller, and P. Dietmaier. Physical processes in wheel–rail contact and its implications on vehicle–track interaction. *Vehicle System Dynamics*, 2015. article in press.

[9] V.L. Popov, S.G. Psakhie, E.V. Shilko, A.I Dmitriev, K. Knothe, F. Bucher, and M. Ertz. Friction coefficient in r̈ail–wheel¨contacts as a function of material and loading parameters. *Physical Mesomechanics*, 5(3):17–24, 2002.

[10] Chiara Modenese. *Numerical Study of the Mechanical Properties of Lunar Soil by the Discrete Element Method*. PhD thesis, University of Oxford, 2013.

[11] V. Šmilauer, E. Catalano, B. Chareyre, S. Dorofeenko, J. Duriez, A. Gladky, J. Kozicki, C. Modenese, L. Scholtès, L. Sibille, J. Stránský, and K. Thoeni. Yade documentation, 2010. The Yade Project, 1st ed., 2010.